nature communications

Article

https://doi.org/10.1038/s41467-025-59910-z

Temperature dependency of energy shift of excitonic states in a donor–acceptor type TADF molecule

Received: 25 March 2024

Accepted: 8 May 2025

Published online: 23 May 2025

Check for updates

Youichi Tsuchiya[1] ✉, Keito Mizukoshi[1,2], Masaki Saigo[3], Tomohiro Ryu[3], Keiko Kusuhara[1], Kiyoshi Miyata[3], Ken Onda[3] & Chihaya Adachi[1,2,4] ✉

In recent years, thermally activated delayed fluorescence (TADF) has attracted intense attention owing to its straightforward application to high-efficiency organic light-emitting diodes. Further, to develop high-performance TADF materials, many researchers have designed novel molecules that have a small energy gap between the lowest excited singlet and triplet states (ΔE_{ST}), and detailed analysis suggests a significant contribution of higher-lying excited states for spin flipping processes. In this study, we demonstrate a peculiar thermal behaviour of emission decay of a donor–acceptor type TADF molecule, **TMCz-BO**, which seems like thermal deactivation of delayed fluorescence that can be explained without a negative ΔE_{ST} by comprehensive kinetic analysis across various temperatures and solvents. While the activation energy has previously been treated as being temperature-independent, we stress that it should be a dynamic parameter affected by changing the solvent-solute interaction with the environmental temperature, especially in the case of a small energy gap.

Through the extensive development of novel organic emitters in organic light-emitting diodes (OLEDs), the singlet and triplet energy levels have been controlled by designing novel molecules. In recent years, thermally activated delayed fluorescence (TADF) materials have been a hot topic, and significant development has been achieved owing to their high applicability for OLEDs with the ultimate quantum efficiency from electrons/holes to photons without using precious metals. TADF materials show unique exciton decay processes, such as bi-exponential decay with a dual lifetime in the nanosecond range and micro to millisecond range originating from the forward and reverse intersystem crossing (ISC and RISC) processes between the lowest singlet (S_1) and lowest triplet (T_1) excited states[1,2]. One of the key issues for efficient TADFs is a small energy gap between the S_1 and T_1 states (ΔE_{ST}) by controlling the highest occupied and lowest unoccupied molecular orbitals[3–7]. Several groups have developed advanced TADF materials with near zero ΔE_{ST} (ZE_{ST}, i.e., 0 ± 25 meV) achieving a short exciton lifetime (τ) of less than 1 μs[8–10]. Because of the presence of activation energies for both the ISC and RISC, they show clear double exponential decay. Interestingly, some unusual TADF behaviours have recently been reported. Yersin et al. designed a novel ZE_{ST} material that showed single-exponential emission decay (τ = 431 ns), and they confirmed the promising OLED characteristics with a high external quantum efficiency of 18.7%[8]. They proposed the ZE_{ST} mechanism based on the significant mixing between the charge transfer (CT) and local excited (LE) states. Further, Aizawa et al. reported experimentally observed negative ΔE_{ST} on a heptazine derivative, **HzTFEX$_2$**[9]. While **HzTFEX$_2$** showed delayed emission with τ = 217 ns at 300 K, shorter delayed emission (τ_d = 195 ns) was confirmed at 200 K in a toluene (TOL) solution. They interpreted these observations as inverted rate constants between the ISC and RISC (i.e., $k_{RISC} > k_{ISC}$) to explain the inverted S_1–T_1 energy state ($InvE_{ST}$). In general, Hund's rule states that a T_1 state has lower energy than a S_1 state[11]. However, azaphenalenes,

[1]Center for Organic Photonics and Electronics Research (OPERA), Kyushu University, Nishi, Fukuoka, Japan. [2]Department of Applied Chemistry, Kyushu University, Nishi, Fukuoka, Japan. [3]Department of Chemistry, Faculty of Science, Kyushu University, Nishi, Fukuoka, Japan. [4]International Institute for Carbon Neutral Energy Research (I2CNER), Kyushu University, Nishi, Fukuoka, Japan. ✉e-mail: tsuchiya@opera.kyushu-u.ac.jp; adachi@opera.kyushu-u.ac.jp

including heptazines, have been confirmed to show an $InvE_{ST}$ by ab initio calculation considering the doubly excited state configuration[12]. Recently, materials with an $InvE_{ST}$ have attracted research interest, and several groups have reported the possibility of $InvE_{ST}$ materials from both theoretical calculations and experiments[13–19].

In 2020, our group reported a cutting-edge TADF emitter with 1,3,6,8-tetramethyl-9*H*-carbazole as the donor unit and 5,9-dioxa-13b-boranaphtho[3,2,1-de]anthracene as the acceptor unit (**TMCz-BO**, Fig. 1a) that showed very short transient decay of 750 ns and high photoluminescence quantum yield (PLQY, 96%) in a 6 wt%-**TMCz-BO**:2,8-bis(diphenylphosphine oxide)dibenzofuran (**PPF**) film[10]. In addition, a very small ΔE_{ST} of 20 meV was estimated from the temperature dependency of its transient photoluminescence (PL) (Supplementary Fig. 1). Considering the high device performance (external quantum efficiency of 20.7%) and the temperature dependence of the transient PL (TRPL) decay, the emission mechanism was assigned as TADF. However, when we investigated the temperature dependence of the delayed emission in various solutions, we observed thermally deactivated behaviour in the delayed emission similar to that of **HzTFEX$_2$** (Fig. 1b). This strongly suggests we should check carefully to understand our result. Here, we report the peculiar temperature dependence of the emission characteristics of **TMCz-BO** that can be explained in the usual TADF framework by our original model including the equilibrium of the T_1 and higher-lying triplet (T_n) states with considering the exciton thermo-dynamics.

Results

S_1–T_1 energy gap estimation

The absorption, fluorescence (at room temperature, rt), and phosphorescence (at 77 K) spectra of **TMCz-BO** in TOL and dichloromethane (DCM) are shown in Fig. 1d. The results in tetrahydropyran (THP), tetrahydrofuran (THF), and acetone (ACE) are summarized in Supplementary Fig. 2. The ΔE_{ST} value in TOL was estimated to be 7 meV with the S_1 and T_1 energy levels of 3.04 and 3.03 eV, respectively, from the spectral onset of the fluorescence and phosphorescence spectra. While **TMCz-BO** showed strong solvatochromism in the fluorescence spectrum, no significant difference was observed in the phosphorescence onset values. Therefore, we obtained negative ΔE_{ST} values in highly polar solvents using these spectral onset values (e.g., −0.23 eV in DCM) (Supplementary Table 1). Because there are several

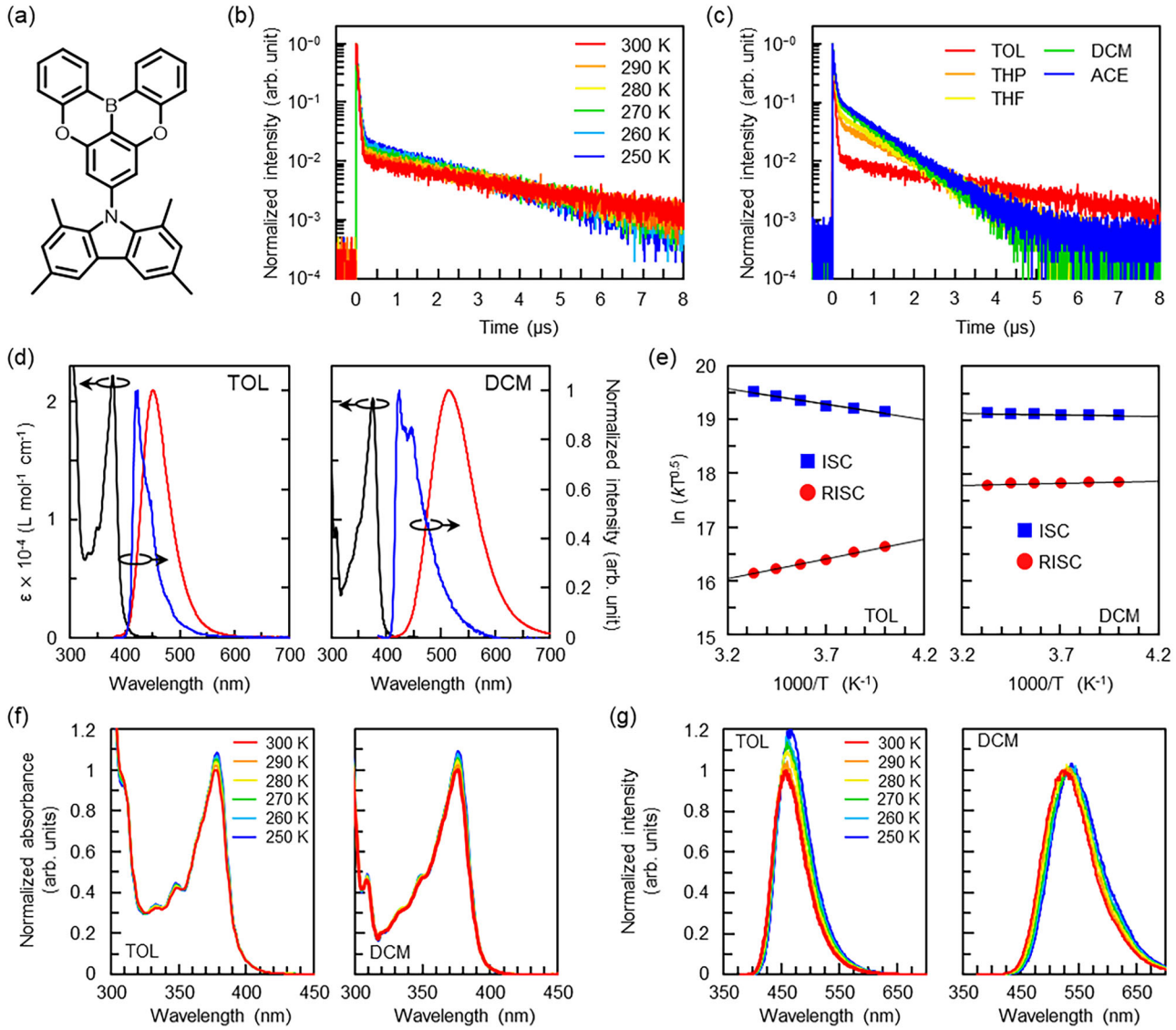

Fig. 1 | Photophysical properties of TMCzBO. a Chemical structure of **TMCz-BO**. **b** Temperature-dependent transient PL decay in TOL, **c** transient PL decay in various solvents, **d** Absorption (black line), fluorescence (rt, red line), and phosphorescence (77 K, blue line) in TOL and DCM, **e** Marcus plots for k_{ISC} and k_{RISC} in TOL and DCM, **f** Temperature-dependent absorption spectra normalized with 300 K, **g** Temperature-dependent emission spectra normalized with 300 K; [**TMCz-BO**] = 2.0×10^{-5} mol L^{-1}.

problems in the estimation of the excited energy from the spectral onset, it is not suitable to discuss the accurate energy levels for TADF materials, particularly those with small energy differences (see Supplementary Notes), e.g., ignoring the energy relaxation at ground (S_0) state, the accuracy of onset value, the solvation in different state of the solvent, inhibition of reorganization at a frozen state, and violation of Kasha's rule[20–22]. Especially, the liner or log scaling for emission intensity makes a large difference in estimated energies (Supplementary Fig. 3 and Supplementary Table 2). In the case of TADF materials, more accurate ΔE_{ST} values can be obtained from the temperature dependence of the emission decay curves. The Arrhenius plot for the estimated ISC (k_{ISC}) and RISC rate constants (k_{RISC}) provides the activation energies (E_a). Subtracting the E_a for RISC (E_a^{RISC}) to ISC processes (E_a^{ISC}), ΔE_{ST} can be estimated[23]. Because the Arrhenius plot drifts by the temperature based on the Marcus equation (Supplementary Eq. (3)), it is suitable to employ the Marcus plot, a corrected Arrhenius plot, to estimate E_a^{ISC} and E_a^{RISC} for TADF materials (see Supplementary Notes)[24].

The TRPL decay of **TMCz-BO** in TOL (Fig. 1b) showed the shortening of a delayed lifetime ($\tau_d = 1/k_d$) with an increased delay component (Φ_{DF}) to the prompt component (Φ_{PF}) by decreasing the temperature; τ_d = 1.02 and 1.86 μs and Φ_{PF}/Φ_{DF} = 0.863 and 0.834 for 250 and 300 K, respectively. This behaviour is opposite from that of **TMCz-BO** in a **PPF** film, where τ_d increased by decreasing the temperature, which is typical TADF behaviour (Supplementary Fig. 1). **TMCz-BO** showed clear bi-exponential decay in TOL. Thus, we applied a typical three-state analysis with the approximation of no triplet radiative decay to a ground state[25]. As a result, the k_{ISC} and k_{RISC} were estimated to be 1.28×10^7 and 1.06×10^6 s^{-1} at 250 K and 1.72×10^7 and 0.59×10^6 s^{-1} at 300 K, respectively (Supplementary Table 3). These results suggest that the ISC is a thermally activated process, whereas the RISC is a thermally deactivated process. Because of its high PLQY in toluene (1.000 and 0.845 at 250 and 300 K, respectively, Supplementary Table 4), it is difficult to explain this by the difference of the nonradiative paths from S_1 or T_1. To confirm the estimation difference of the nonradiative paths, the possible ranges of the rate constants are summarized in Supplementary Table 3.

The emission decay of **TMCz-BO** also showed strong solvent polarity dependence (Fig. 1c and Supplementary Figs. 4 and 5). Longer delayed emission τ_d was observed in lower polarity solvents for each temperature (Supplementary Table 5). The Marcus plots of **TMCz-BO** in TOL and DCM are shown in Fig. 1d. The data for all five solvents are summarized in Supplementary Fig. 6 and Supplementary Table 6 including the results of Arrhenius plot analysis (all data in HEX, MES and PC, where **TMCzBO** showed low PLQY, are summarized in Supplementary Figs. 7–9 and Supplementary Tables 7 and 8 as just for information). Here, a negative ΔE_{ST} value of −114 meV was estimated in TOL based on E_a^{ISC} and E_a^{RISC} of 49 and −65 meV, respectively. Moreover, the ΔE_{ST} values were negative in all of the five solvents. The ΔE_{ST} values of −12 and −5 meV in DCM and ACE were provided those negative E_a^{RISC} meanwhile the conventional TADF-like thermal behaviour was provided. Generally, bi-exponential exciton decay can be explained by a three-state model[26]. However, it is difficult to explain the unique thermal behaviour of **TMCz-BO** by a three-state model even when the $InvE_{ST}$ energy arrangement is taken into consideration. Furthermore, although $k_{RISC} > k_{ISC}$ is considered strong evidence for $InvE_{ST}$ material[9], k_{ISC} was always greater than k_{RISC} in all solvents investigated in the case of **TMCz-BO**.

Next, we investigated the participation of the dark states in the transient absorption spectra at 250 and 300 K (Supplementary Fig. 10). The exciton lifetime was found to show a similar trend to the TRPL in both TOL and DCM. Therefore, we conclude that it is difficult to discuss the contribution of additional dark states that cannot be detected in the TRPL. Further, a post-Hartree–Fock calculation considering the doubly excited states at the SCS-CC2/def2-TZVP level of theory suggested a positive ΔE_{ST} of 0.20 eV (Supplementary Table 9). A time-dependent density functional theory calculation at the ωB97X-D/6-31 G(d,p) level of theory gave similar results. Thus, both the transient absorption spectra and advanced calculations did not provide information about the possible mechanism.

Model construction and simulations

The key is the negative E_a^{RISC} obtained from the Marcus plots. Because E_a is an energy barrier for the conversion process from the initial state to the final state, the value must be positive. However, negative E_a values as apparent values are sometimes found in the kinetic analysis of chemical reactions, which can be explained by the presence of an endothermic equilibrium between a precursor chemical as an initial state and another species uninvolved in the reaction[26–29]. Therefore, the negative E_a^{RISC} can also be explained as an apparent value by the presence of an endothermic equilibrium with an upper state that works as a trap state. Thus, we introduced this perspective in the time-dependent exciton decay process. Here, we consider a four-state model, which is explained with a S_0 state, excited singlet and triple CT states (^{1}CT and ^{3}CT), and a triplet LE state (^{3}LE). Here, we assume that the energy level of ^{3}CT is higher than that of ^{3}LE. In this case, the direct spin-flipping process between ^{1}CT and ^{3}CT is inhibited by the El-Sayed rule. When the internal conversion process between ^{3}LE and ^{3}CT is much faster than the RISC process, the exciton distribution between ^{3}LE and ^{3}CT can be explained by the Boltzmann distribution. In fact, the relaxation rate is much faster than the radiative and RISC rates in solution[30]. Thus, the differential equations for this exciton decay process can be expressed as

$$\frac{d[^1\mathrm{CT}]}{dt} = -\left(k_r^S + k_{nr}^S + k_{ISC}\right)[^1\mathrm{CT}] + k_{RISC}[^3\mathrm{LE}], \tag{1}$$

$$\frac{d[T_{total}]}{dt} = k_{ISC}[^1\mathrm{CT}] - k_{RISC}[^3\mathrm{LE}] - \left(k_r^T + k_{nr}^T\right)[T_{total}], \tag{2}$$

$$[T_{total}] = [^3\mathrm{LE}] + [^3\mathrm{CT}], \tag{3}$$

$$\frac{[^3\mathrm{CT}]}{[^3\mathrm{LE}]} = \exp\left[\frac{-(\Delta E_{3CT-3LE})}{k_B T}\right], \tag{4}$$

where k_r^S, k_{nr}^S, k_r^T, and k_{nr}^T are the radiative and nonradiative decay rates from the singlet and triplet states and $\Delta E_{3CT-3LE}$ is the energy gap between ^{3}CT and ^{3}LE. Here, k_r^T and k_{nr}^T are not separated for the ^{3}CT and ^{3}LE states because the two states form a thermal equilibrium by the Boltzmann distribution, and it is difficult to separate these decay processes between ^{3}CT and ^{3}LE. These terms can be removed to ensure consistency with the three-state kinetics under the approximation of no phosphorescence decay. The values of k_{ISC} and k_{RISC} are provided by E_a^{ISC} and E_a^{RISC} using the Marcus equation, respectively. When $\Delta E_{3CT-3LE} < 0$, the condition is the same as the conventional four-state model. The combination of the Boltzmann distribution and the Marcus equation has been used to estimate the theoretical k_{RISC} for the ^{3}CT→^{3}LE→^{1}CT system[21,22].

The theoretical curves obtained from the above model considering exciton trapping (**model 1**) were analysed with the three-state kinetics and Marcus plot, which was the same method used to analyse the experimental results, and the resulting E_a and ΔE_{ST} values from the theoretical model were compared with those of the variables. **Model 1** succeeded in explaining the $InvE_{ST}$-like thermal behaviour of the exciton decay with the excited state energy configuration of conventional TADF (Fig. 2 and Supplementary Table 10). For example, the simulation provided $InvE_{ST}$-like thermal behaviour with the parameters of 1, 2 and 10 meV for E_a^{ISC}, E_a^{RISC}, and $\Delta E_{3CT-3LE}$, respectively (Fig. 2b). In this case, the actual ΔE_{ST} value is 1 meV, but the analysed ΔE_{ST} value

https://doi.org/10.1038/s41467-025-59910-z

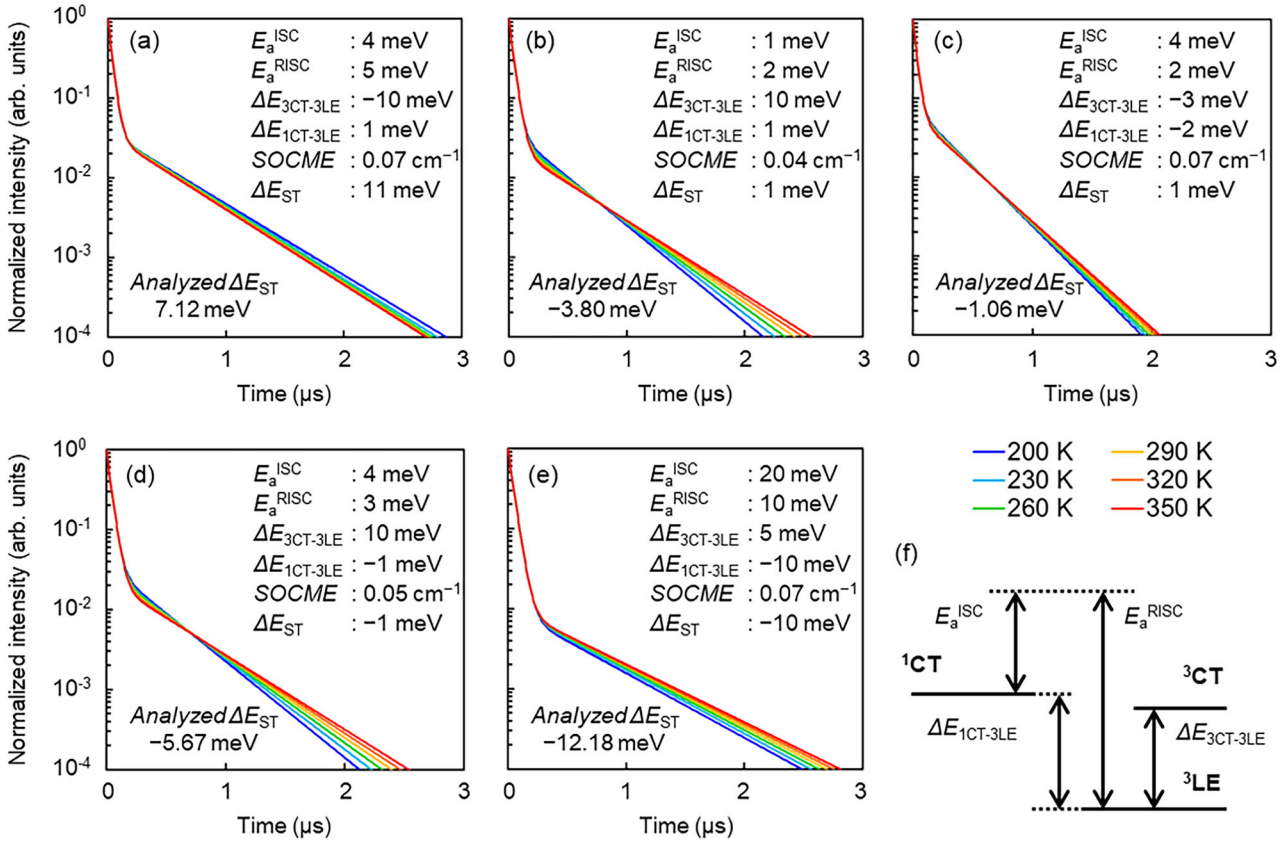

Fig. 2 | Simulated emission decay curves with considering exciton trap. Examples of the decay curves simulated with **model 1** with near zero S_1–T_1 energy splitting (ZE_{ST}); $k_r + k_{nr} = 2 \times 10^7$ s^{-1}. **a**–**c** Conventional TADF energy configuration, (**d**, **e**) $InvE_{ST}$ energy configuration, (**f**) excited state energy diagram showing each energy gap. Analytical results with conventional method showed (**a**) positive ΔE_{ST}, (**b**) negative ΔE_{ST} by $E_a^{ISC} > E_a^{RISC}$, (**c**) negative ΔE_{ST} with negative E_a^{RISC}, (**d**) negative ΔE_{ST} with negative E_a^{RISC}, (**e**) negative ΔE_{ST} by $E_a^{ISC} > E_a^{RISC}$. (See Supplementary Fig. 10 for other energy configurations including non-ZE_{ST} ones.).

was −3.80 meV with a negative E_a^{RISC} of −1.89 meV. Interestingly, the energy region of $0 \le \Delta E_{ST} < 10$ meV provides the apparent negative ΔE_{ST} with positive E_a^{ISC} and E_a^{RISC} even in the energy configuration of conventional TADF (Fig. 2c). The analysed values of E_a^{ISC}, E_a^{RISC}, and ΔE_{ST} were 4.80, 3.74 and −1.06 meV when the parameters were 4, 2 and −3 meV for E_a^{ISC}, E_a^{RISC} and $\Delta E_{3CT-3LE}$, respectively. In this configuration, ^{3}LE is located 2 meV higher than ^{1}CT and ^{3}CT is located 1 meV lower than ^{1}CT. Thus, we confirmed that the negative ΔE_{ST} with the $E_a^{ISC} > E_a^{RISC}$ was present in the regular energy configuration of TADF. Furthermore, we confirmed that the negative ΔE_{ST} with the negative E_a^{RISC} was present in the $InvE_{ST}$ energy configuration (Fig. 2d). More interestingly, a decrease of the delayed fluorescence components at lower temperatures was also obtained in the $InvE_{ST}$ energy configuration (Fig. 2e). These simulation results indicate that care should be taken when analysing the materials in the case of negative ΔE_{ST} estimated from the thermal behaviour of the emission decay. Thus, the ΔE_{ST} value estimated by the thermal dependence of the rate constants is an apparent value based on the mismatch of the supposed and actual emission mechanisms.

Model improvement to explain the thermal behaviour in various solvents

In the case of **model 1**, the experimental results of **TMCz-BO** could not be well explained even by introducing the different SOC strengths for the ISC and RISC processes because of simplification employing $k_r^S + k_{nr}^S$ as a temperature-independent value. Thus, $k_r^S + k_{nr}^S$ was treated as a temperature-dependent term in **model 2** considering the temperature-dependent PLQY (Supplementary Table 4). The difference between each model is summarized in Fig. 3. While different SOC strengths were required for the ISC and RISC processes to explain the experimental results, **model 2** provided better fitting (Table 1 and Supplementary Tables 11 and 12). Here, this still suggests the $InvE_{ST}$ energy configuration for **TMCz-BO**. The ΔE_{ST} values were −112 and −0.5 meV in TOL and DCM, respectively. In addition, the SOC strength for the ISC process in TOL was very large (1.358 cm^{-1}). Thus, **model 2** is not a suitable model to explain the energy arrangement of **TMCz-BO**.

Next, we focused on the onset value of the absorption spectrum, which did not show temperature dependence, while that of the emission spectrum showed a slight red shift in all of the solvents at lower temperatures (Supplementary Figs. 11 and 12). This is not unique to **TMCz-BO**, and it is an often-reported phenomenon[31]. This red-shifted emission indicates that the excited states were stabilized by the increased solvent polarity by decreasing the temperature, which can be described by the Onsager model of dielectrics[32]. The experimental results can be explained based on the larger dipole moment than the ground state in the CT excited states of donor–acceptor-type molecules, lowering ^{1}CT and ^{3}CT. To fit the temperature dependence of the CT energies, we introduced the following equation for both the ISC and RISC processes:

$$E_a = E_a^{300} + \Delta E_a^T (300 - T) \quad (5)$$

where E_a^{300} is the activation energy at 300 K and ΔE_a^T is the E_a shift coefficient for the temperature difference. Note that E_a has been estimated from the temperature dependence of the rate constant under the assumption that it has no temperature dependence in most of the previous reports. However, the temperature dependency of E_a on electron transfer have been reported[33]. When the ^{1}CT energy shift

https://doi.org/10.1038/s41467-025-59910-z

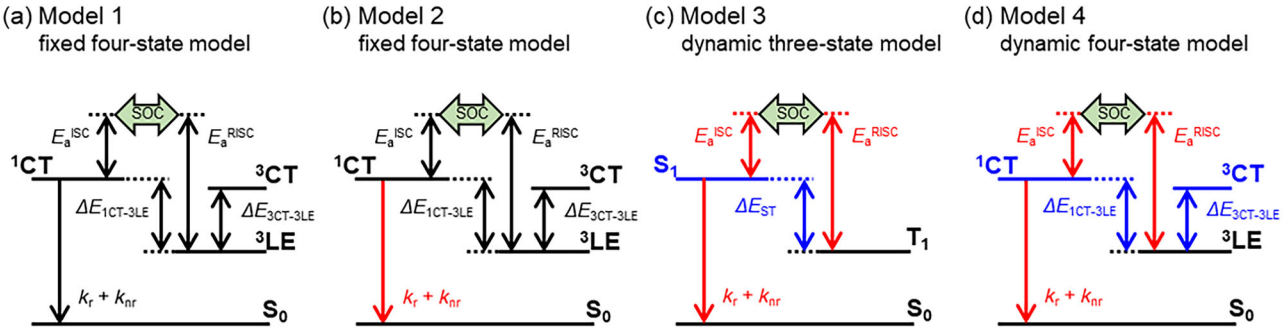

Fig. 3 | Schematic energy diagrams. a model 1, b model 2, c model 3 and **d model 4**. E_a^{ISC} and E_a^{RISC} should be ≥0, but $\Delta E_{1CT-3LE}$ and $\Delta E_{3CT-3LE}$ can be both positive and negative. Red-coloured fitting parameters have temperature dependence, and the blue-coloured energies are shifted by temperature dependency of red-coloured fitting parameters.

Table 1 | Estimated energy configuration by model fitting and the results of Marcus plot in the three-state system analysed for fitting curves by each model

Solvents	Fitting parameter for each model				Analysed values with Marcus plot		
	E_a^{ISC} (meV)	E_a^{RISC} (meV)	$E_{3CT-3LE}$ (meV)	ΔE_{ST} (meV)	E_a^{ISC} (meV)	E_a^{RISC} (meV)	ΔE_{ST} (meV)
Experimental value							
TOL	–	–	–	–	49.0	−65.0	−114.0
DCM	–	–	–	–	4.1	−7.0	−11.6
model 2							
TOL	111.7	0.0	30.0	−111.7	81.5	−2.9	−84.4
DCM	0.7	0.2	27.0	−0.5	4.1	−6.6	−10.6
model 3							
TOL	55.5[a]	140.0[a]	–	84.6[a]	48. 7	−64.8	−113.5
DCM	36.4[a]	68.9[a]	–	32.6[a]	3.8	−7.6	−11.3
model 4							
TOL	10.1[a]	93.2[a]	69.5[a]	83.1[a]	48.7	−65.2	−113.9
DCM	24.9[a]	26.2[a]	−22.6[a]	23.9[a]	3.9	−7.2	−11.1

[a]At 300 K.

by the temperature is considered, it should also be considered. This means that the analytical E_a values are no longer accurate regardless of the presence or absence of the trap states. Here, we assume that the energy shift has a linear relationship with the temperature shift in the measurement region[34]. In **model 3**, we ignored the trap state, i.e., there is no exciton equilibrium in the triplet state (the Boltzmann distribution between ^{3}LE and ^{3}CT is not considered) but included the temperature dependence of the ^{1}CT energy and the PLQY. This does not mean that $\Delta E_{3CT-3LE} = 0$ in Eq. (4) but $[^3\mathrm{LE}] = [T_{total}]$ in Eqs. (1) and (2), i.e., the absence of the trap state. The experimental curves were well explained by **model 3** in all of the solvents, including TOL and THP. ΔE_{ST} increased with increasing temperature in all of the solvents. For example, ΔE_{ST} = 85 and 52 meV in TOL and ΔE_{ST} = 33 and 26 meV in DCM for 300 and 250 K, respectively (Supplementary Tables 11 and 12). However, **model 3** provided a larger SOC strength for an activation state of ISC and RISC in lower polarity solvent: SOCME = 0.547, 0.487, 0.479, 0.274 and 0.142 cm^{-1} for TOL, THP, THF, DCM and ACE, respectively; note that, it was difficult to find the value for global minimum when the assuming SOCME is independent to solvent were employed (see Supplementary Notes). Thus, there were significant differences despite there being no external heavy atom effect. While **model 3** explained the temperature dependence of the emission decay curves of the experimental results very well, it is insufficient to explain why **TMCz-BO** in TOL showed a large ΔE_{ST} decrease by decreasing the temperature (Supplementary Fig. 13).

Comprehensive analysis across various temperatures and solvents with a dynamic four-state model

Model 4 considered the trap state again, in addition to the temperature dependence for both the solvent polarity and nonradiative decay processes. Because the relative energy of each excited state should change with the temperature, the temperature dependence (ΔE^T_{CT-LE}) for the energy difference of ^{3}CT and ^{3}LE ($\Delta E_{3CT-3LE}$ in Eq. (4)) was also introduced:

$$\Delta E_{3CT-3LE} = \Delta E^{300}_{3CT-3LE} + \Delta E^{T}_{3CT-3LE}(300 - T) \tag{6}$$

Because the time constant for solvation is faster than the rate constants related to exciton decay[35], it is possible to assume there is a similar magnitude of solvation effect both in ^{1}CT and ^{3}CT states[36,37]. Therefore, the following approximation was used to decrease the arbitrary parameters:

$$\Delta E^T_{3CT-3LE} \approx \Delta E^T_{a,RISC} - \Delta E^T_{a,ISC} \tag{7}$$

Here, the right-hand side of the equation corresponds to the variation of the ^{1}CT and ^{3}LE levels based on Supplementary Eq. (2) and Eq. (5). Further, the effect of the solvent polarity on the SOC strength can be ignored because there is no heavy atom effect. The SOC strength was estimated to be 0.186 cm^{-1} by comprehensive fitting using all of the decay curves under different conditions. This value is similar to the reported SOC strength determined by the DFT calculation of 0.127 cm^{-1}[10].

In **model 4**, the fitting results for all the solvents well explained the experimental results, and the results of the conventional three-state kinetic analysis applying to the obtained theoretical curves showed good agreement between the experimental and theoretical bi-exponential emission decay curves (Fig. 4a, Supplementary Fig. 14 and Supplementary Tables 11–13). The actual ΔE_{ST} of **TMCz-BO** estimated from the fitting parameters still showed a large decrease with decreasing temperature in TOL and THP, while that in THF, DCM and ACE showed no temperature dependence (Fig. 4b). Similar to **model 3**, the ΔE_{ST} values showed positive values for all of the conditions. This behaviour can be clearly explained by the temperature dependence of each excited state. The temperature dependence of the energy differences of ^{1}CT–^{3}LE and ^{3}CT–^{3}LE for each solvent is shown in Supplementary Fig. 15. The slopes were less than −1 meV K^{-1} with a smaller slope in higher solvent polarity: slopes of −0.70, −0.56, −0.50, −0.45 and −0.44 meV K^{-1} for TOL, THP, THF, DCM and ACE, respectively. While the ^{1}CT–^{3}LE gaps for TOL and THP were always positive under the investigated conditions, the ^{3}CT–^{3}LE gaps for THF, DCM and ACE were negative. In the case of THP, the gap was negative below 280 K, which can be confirmed as the inflection point at approximately 280 K in Fig. 4b. The energies of ^{1}CT and ^{3}CT continuously decreased with

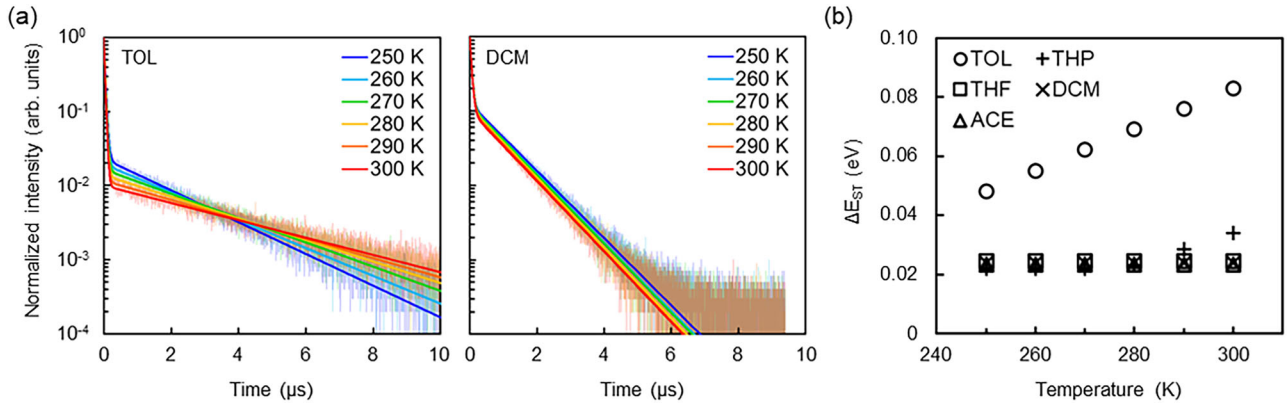

Fig. 4 | Comprehensive fitting results with model 4 for experimental PL decay of TMCz-BO. a Experimental PL decay and fitting curves in TOL and DCM. **b** Temperature-dependent energy configuration estimated by **model 4**.

increasing solvent polarity (Supplementary Fig. 16). The analytical results for the fitting curves obtained by the Marcus plot based on the three-state model agreed well with those of the experimental data analysis (Table 1 and Supplementary Table 14). The reliability of comprehensive analysis result with the dynamic four-state model was confirmed with the temperature dependence decay data of **TMCz-BO** in TOL for 200–250 K by using the obtained fitting parameters for 250–300 K (Supplementary Fig. 17). Therefore, this method is enough to explain the photophysics of solution state even in the low temperature. As explained above, the analysis with **model 4** revealed that **TMCz-BO** has a small ΔE_{ST} exciton energy configuration, like conventional TADF. The dependence of the energy shift of the excitonic states on the temperature provides the peculiar thermal behaviour, like an $InvE_{ST}$ material, in the emission decay of **TMCz-BO**. Based on the analytical result of the dynamic four-state model, $\Delta E_{3CT-3LE}$ values were ca. 70 and 35 meV at 300 and 250 K, respectively, and the population of ^{3}LE is 94 and 83%. This 10% difference would provide few spectral differences in the transient absorption spectra (Supplementary Fig. 10).

Discussion

In this study, we studied the peculiar thermal behaviour of a TADF material, **TMCz-BO**, that shows faster delayed emission at lower temperatures in the solution state. The dynamic four-state model considering the temperature dependence of the solvent polarity (**model 4**) well explained the decay process, which can be ascribed to the different energy configurations of the excited states. Finally, we conclude that **TMCz-BO** is a material showing an apparent negative ΔE_{ST} of −114 meV based on the conventional analytical method but it has positive ΔE_{ST}. The important findings are the contribution of higher-lying triplet state and the thermal dependency of activation energy, which is believed to be a temperature-independent constant in general. The excited-state energy configurations have been experimentally estimated so far, but it has not been so accurate. The comprehensive analytical method with dynamic exciton model can provide higher-resolution analytical results, especially in the small energy gap of ΔE_{ST}. Our findings do not repudiate **HzTFEX$_2$** as an $InvE_{ST}$ material. However, a recent report states that $InvE_{ST}$ needs to be carefully explained theoretically[38]. Most of the theoretical research on $InvE_{ST}$ does not consider the solvation effect and higher-order excited state configurations than doubly-excited configurations. Also, the experimental evidence should be carefully examined to clarify the violation of Hund's rule experimentally. The rate constants should be discussed not only under the mathematically reasonable condition of $k_{nr}^T = 0$, but also for $k_{nr}^S = 0$, as pointed out in our previous report[25]. In fact, the ranges of k_{ISC} and k_{RISC} for **HzTFEX$_2$**, which has been reported to be an $InvE_{ST}$ material with $k_{RISC} > k_{ISC}$ in the case of $k_{nr}^T = 0$, are $(4.61 \mp 1.94) \times 10^7$ and $(4.07 \pm 0.07) \times 10^7\ s^{-1}$, respectively[9,25]. $k_{RISC} < k_{ISC}$ under the condition of $k_{nr}^S = 0 (k_{ISC} = 6.55 \times 10^7\ s^{-1}$ and $k_{RISC} = 4.00 \times 10^7\ s^{-1})$. Therefore, it is desirable to investigate the temperature dependence of the TRPL decay in various solvents for the reported $InvE_{ST}$ materials or candidates and to comprehensively analyse the experimental results, which will open a new stage to develop the advanced TADF emitters. Furthermore, it is very important to apply the comprehensive kinetic analysis using the dynamic four-state model to existing and novel TADF materials, such as multiple resonant- and high-performance TADF materials to experimentally obtain their higher-resolution descriptions of excited state energies. This will not only help us understand the actual emission mechanism of TADF due to the dynamic energy configuration of excitons but also be useful for developing further high-performance TADF in combination with computational quantum calculations. Although it may not be necessary to apply the dynamic three-level or four-level model always through the TADF materials development cycle, it is important to keep in mind and discuss that the exciton energy levels are dynamic, and the estimated energies are the apparent values.

Methods

General information

TMCz-BO was synthesized by a previously reported method[10]. The photophysical measurements were performed using a tightly closed cell with a greaseless Teflon valve. The PLQY was checked, and there was no significant error (<3%) before and after the temperature-dependence measurement. The phosphorescence measurement was performed using an NMR glass tube. The transient emission decay was measured by a Quantaurus-Tau fluorescence lifetime measurement system (C11367, Hamamatsu, Japan) and a streak camera system (C10910, Hamamatsu) with a Nd-YAG third-harmonic laser (PL-2251, ESPKLA, Lithuania). The fluorescence and phosphorescence were measured with an FP-8600 spectrofluorometer (JASCO, Japan). The absorption spectra were measured with a Lambda 950 spectrophotometer (Perkin-Elmer, USA). The absolute PLQY was measured with a Quantaurus-QY PLQY spectrometer (C11347, Hamamatsu). For all of the photophysical measurements, the temperature was controlled by a CoolSpeK cryostat (Unisok, Japan). The computational calculations were performed with Gaussian16 Rev.A.03 and TURBOMOL 7.21[39].

Solvent polarity

The fundamental photophysical properties of the absorption, fluorescence (at rt), and phosphorescence (at 77 K) spectra, PLQY, and TRPL were investigated in *n*-hexane (HEX, 30.9), mesitylene (MES, 32.9), TOL (33.9), THP (36.2), THF (37.5), DCM (40.7), ACE (42.3), and propylene carbonate (PC, 46.0). The values in parentheses are the solvent polarity indicator in $E_T(30)$ for each solvent (in kcal mol^{-1})[40]

Because of the very low PL intensity of **TMCz-BO** in HEX, MES, and PC (< 0.50% PLQY, Supplementary Table 1), we focused on the other five solvents.

Estimation of the relative PLQY

The relative PLQYs at low temperature were estimated using the absorption and emission for light excitation at each temperature by

$$\Phi_{PLQY}^{T} = \frac{\Phi_{PLQY}^{300} R_{FL}^{T}}{R_{Abs}^{T}} = \Phi_{PLQY}^{300} \frac{P_{FL}^{T}}{P_{FL}^{300}} \cdot \frac{P_{Abs}^{300}}{P_{Abs}^{T}} \tag{8}$$

$$P_{Abs}^{T} = \sum \alpha^{T} N_{photon}^{Ex} = \sum \left(1 - \frac{1}{10^{A^{T}}}\right) N_{photon}^{Ex} \tag{9}$$

where Φ_{PLQY}^{T} is the relative PLQY at each temperature, Φ_{PLQY}^{300} is the absolute PLQY measured at 300 K, R_{Abs}^{T} and R_{FL}^{T} are the relative photon numbers of the absorption and emission for 300 K, P_{PL}^{T} and P_{PL}^{300} are the detected emitted photon numbers at each temperature and 300 K, P_{Abs}^{T} and P_{Abs}^{300} are the total absorbed photon numbers for the irradiated photons (normalized) at each temperature and 300 K, α^{T} and A^{T} are the absorption ratio and absorbance at each temperature and each wavelength, and N_{photon}^{Ex} is the irradiated photon number for each wavelength normalized by the peak maximum of the excitation light spectrum.

Fitting details

The curve fitting was performed by chi-square fitting assuming the variance is 1 using Microsoft Excel with the GRG nonlinear solving method. The reduced chi-square χ_{ν}^{2} was used to check the goodness of fit eliminating the plots with the experimental data of 0. The model fitting by each model was performed for all of the experimental temperature-dependent emission decays for each solvent. In the case of **model 4**, the SOC matrix element (SOCME) was estimated as a global minimum by the fitting error investigation for the comprehensive fitting over the various temperature and solvent. A small data set, which explains the trend of the environment dependence for PF and DF from the bi-exponential fitting curves of the experimental data, was used instead of the full experimental data to eliminate the error on data collection which have a possibility to trap to the local minimum. The χ_{ν}^{2} of the model fitting to the full experimental data were provided with the additional fitting only for the baseline.

Data availability

All data generated in this study are provided in the Supplementary Information.

References

1. Uoyama, H. et al. Highly efficient organic light-emitting diodes from delayed fluorescence. *Nature* **492**, 234–238 (2012).
2. Endo, A. et al. Efficient up-conversion of triplet excitons into a singlet state and its application for organic light emitting diodes. *Appl. Phys. Lett.* **98**, 083302 (2011).
3. Liu, Y., Li, C., Ren, Z., Yan, S. & Bryce, M. R. Highly twisted thermally activated delayed fluorescence (TADF) molecules and their applications in organic light-emitting diodes (OLEDs). *Angew. Chem. Int. Ed.* **62**, e202301896 (2023).
4. Liu, Y., Li, C., Ren, Z., Yan, S. & Bryce, M. R. All-organic thermally activated delayed fluorescence materials for organic light-emitting diodes. *Nat. Rev. Mater.* **3**, 18020 (2018).
5. Im, Y. et al. Molecular design strategy of organic thermally activated delayed fluorescence emitters. *Chem. Mater.* **29**, 1946–1963 (2017).
6. Wong, M. Y. & Zysman-Colman, E. Purely organic thermally activated delayed fluorescence materials for organic light-emitting diodes. *Adv. Mater.* **29**, 1605444 (2017).
7. Dias, F. B., Penfold, T. J. & Monkman, A. P. Photophysics of thermally activated delayed fluorescence molecules. *Methods Appl. Fluoresc.* **5**, 012001 (2017).
8. Yersin, H., Mataranga-Pora, L., Czerwieniec, R. & Dovbii, Y. Design of a new mechanism beyond thermally activated delayed fluorescence toward fourth generation organic light emitting diodes. *Chem. Mater.* **31**, 6110–6116 (2019).
9. Aizawa, N. et al. Delayed fluorescence from inverted singlet and triplet excited states. *Nature* **609**, 502–506 (2022).
10. Kim, J. U. et al. Nanosecond-time-scale delayed fluorescence molecule for deep-blue OLEDs with small efficiency rolloff. *Nat. Commun.* **11**, 1765 (2020).
11. Hund, F. Zur Deutung verwickelter Spektren, insbesondere der Elemente Scandium bis Nickel. *Z. Phys.* **33**, 345–371 (1925).
12. Leupin, W. & Wirz, J. Low-lying electronically excited states of cycl[3.3.3]azine, a bridged 12π-perimeter. *J. Am. Chem. Soc.* **102**, 6068–6075 (1980).
13. Ehrmaier, J. et al. Singlet–triplet inversion in heptazine and in polymeric carbon nitrides. *J. Phys. Chem. A* **123**, 8099–8108 (2019).
14. de Silva, P. Inverted singlet–triplet gaps and their relevance to thermally activated delayed fluorescence. *J. Phys. Chem. Lett.* **10**, 5674–5679 (2019).
15. Sanz-Rodrigo, J., Ricci, G., Olivier, Y. & Sancho-Garcia, J.-C. Negative singlet–triplet excitation energy gap in triangle-shaped molecular emitters for efficient triplet harvesting. *J. Phys. Chem. A* **125**, 513–522 (2021).
16. Ricci, G., San-Fabián, E., Olivier, Y. & Sancho-García, J.-C. Singlet-triplet excited-state inversion in heptazine and related molecules: assessment of TD-DFT and ab initio methods. *Chem. Phys. Chem.* **22**, 553–560 (2021).
17. Pollice, R., Friederich, P., Lavigne, C., dos Passos Gomes, G. & Aspuru-Guzik, A. Organic molecules with inverted gaps between first excited singlet and triplet states and appreciable fluorescence rates. *Matter* **4**, 1654–1682 (2021).
18. Sobolewski, A. L. & Domcke, W. Are heptazine-based organic light-emitting diode chromophores thermally activated delayed fluorescence or inverted singlet–triplet systems? *J. Phys. Chem. Lett.* **12**, 6852–6860 (2021).
19. Audebert, P., Kroke, E., Posern, C. & Lee, S.-H. State of the art in the preparation and properties of molecular monomeric s-heptazines: syntheses, characteristics, and functional applications. *Chem. Rev.* **121**, 2515–2544 (2021).
20. Auffray, M., Balijapalli, U., Ribierre, J.-C., Tsuchiya, Y. & Adachi, C. Sub-microsecond TADF emission in D-D′-A emitters. *Chem. Lett.* **49**, 932–935 (2020).
21. Qiao, X. et al. Upper excited triplet state-mediated intersystem crossing for anti-kasha's fluorescence: potential application in deep-ultraviolet sensing. *J. Phys. Chem. C.* **123**, 5761–5766 (2019).
22. Sato, T., Uejima, M., Tanaka, K., Kaji, H. & Adachi, C. A light-emitting mechanism for organic light-emitting diodes: molecular design for inverted singlet–triplet structure and symmetry-controlled thermally activated delayed fluorescence. *J. Mater. Chem. C.* **3**, 870–878 (2015).
23. Noda, H. et al. Critical role of intermediate electronic states for spin-flip processes in charge-transfer-type organic molecules with multiple donors and acceptors. *Nat. Mater.* **18**, 1084–1090 (2019).
24. Bae, J. et al. Multiple resonance type thermally activated delayed fluorescence by dibenzo[1,4]azaborine derivatives. *Front. Chem.* **10**, 990918 (2022).
25. Tsuchiya, Y. et al. Exact solution of kinetic analysis for thermally activated delayed fluorescence materials. *J. Phys. Chem. A* **125**, 8074–8089 (2021).
26. Atkins, P. W., Paula, J. & Keeler, J. *Physical Chemistry* (11th ed.). 750 (Oxford University Press, 2018).

27. Mozurkewich, M. & Benson, S. W. Negative activation energies and curved arrhenius plots: 1. Theory of reactions over potential wells. *J. Phys. Chem.* **88**, 6429–6435 (1984).
28. Mozurkewich, M., Lamb, J. J. & Benson, S. W. Negative activation energies and curved arrhenius plots: 2. Hydroxyl + carbon monoxide. *J. Phys. Chem.* **88**, 6435–6441 (1984).
29. Lamb, J. J., Mozurkewich, M. & Benson, S. W. Negative activation energies and curved arrhenius plots: 3. Hydroxyl + nitric acid and hydroxyl + peroxynitric acid. *J. Phys. Chem.* **88**, 6441–6448 (1984).
30. Gillett, A. J. et al. Dielectric control of reverse intersystem crossing in thermally activated delayed fluorescence emitters. *Nat. Mater.* **21**, 1150–1157 (2022).
31. Etherington, M. K., Gibson, J., Higginbotham, H. F., Penfold, T. J. & Monkman, A. P. Revealing the spin–vibronic coupling mechanism of thermally activated delayed fluorescence. *Nat. Commun.* **7**, 13680 (2016).
32. Suppan, P. & Tsiamis, C. Temperature effects in solvatochromic shifts. *J. Chem. Soc., Faraday Trans. 2* **77**, 1553–1562 (1981).
33. Jortner, J. Temperature dependent activation energy for electron transfer between biological molecules. *J. Chem. Phys* **64**, 4860–4867 (1976).
34. Mopsik, F. I. Dielectric properties of slightly polar organic liquids as a function of pressure, volume, and temperature. *J. Chem. Phys.* **50**, 2559–2569 (1969).
35. Huu, D. K. A. P. et al. Thermally activated delayed fluorescence: polarity, rigidity, and disorder in condensed phases. *J. Am. Chem. Soc.* **144**, 15211–15222 (2022).
36. Serdiuk, I. E. et al. Vibrationally assisted direct intersystem crossing between the same charge-transfer states for thermally activated delayed fluorescence: analysis by marcus–hush theory including reorganization energy. *J. Phys. Chem. B* **125**, 2696–2706 (2021).
37. Yersin, H. et al. Eliminating the reverse ISC bottleneck of TADF through excited state engineering and environment-tuning toward state resonance leading to mono-exponential sub-µs decay. High OLED external quantum efficiency confirms efficient exciton harvesting. *Adv. Funct. Mater.* **32**, 2201772 (2022).
38. Dreuw, A. & Hoffmann, M. The inverted singlet-triplet gap: a vanishing myth? *Front. Chem.* **11**, 1239604 (2023).
39. Frisch, M. J. et al. Gaussian 16, Revision A.03 (Gaussian, Inc., Wallingford CT, 2016).
40. Cerón-Carrasco, J. P. et al. Solvent polarity scales: determination of new $E_T(30)$ values for 84 organic solvents. *J. Phys. Org. Chem.* **27**, 512–518 (2014).

Acknowledgements

This work was supported by Kyulux Inc. (Y.T. and C.A.), Japan Science and Technology Agency (JST) CREST (grant no. JPMJCR22B3) (C.A.), Ministry of Education, Culture, Sports, Science and Technology (MEXT)/Japan Society for the Promotion of Science (JSPS) KAKENHI Grant Numbers 23H05406 (C.A.), 23K20039 (K.O. and C.A.), 20J21226 (M.S.), 21K14590 (Ki.M.), 23H01977 (K.O.), 23H03833 (Ki.M.), 23H04631 (K.O.), Kyushu University Platform of Inter-/Transdisciplinary Energy Research (Q-PIT) through its "Module-Research Program.", Kyushu University Integrated Initiative for Designing Future Society (T.R.), Sumitomo Basic Science Research Projects (Ki.M.), and JST, the establishment of university fellowships for the creation of science technology innovation, Grant Number JPMJFS2132 (T.R.). The partial computation was carried out using the computer resource offered by Research Institute for Information Technology, Kyushu University. We thank Edanz for editing a draft of this manuscript.

Author contributions

Y.T. conceived the project and designed the initial experiments. Ke.M. performed experiments regarding the steady-state spectroscopy, emission decay property, and photoluminescence quantum yield. M.S, T.R. and Ki.M. performed experiment and analysis regarding the transient absorption. Ke.M. performed computational analysis. K.K. synthesized the material. Y.T. and Ke.M. analysed the data. Y.T., Ki.M, K.O. and C.A. validated analysed results and discussions. Y.T. and C.A. wrote the manuscript. All authors have read and agreed to the published version of the manuscript.

Competing interests

The authors declare no competing interests.

Additional information

Supplementary information The online version contains supplementary material available at https://doi.org/10.1038/s41467-025-59910-z.

Correspondence and requests for materials should be addressed to Youichi Tsuchiya or Chihaya Adachi.

Peer review information *Nature Communications* thanks the anonymous, reviewer(s) for their contribution to the peer review of this work. A peer review file is available.